

Article

Molecular Dynamics Study on the Resonance Properties of a Nano Resonator Based on a Graphene Sheet with Two Types of Vacancy Defects

Wenchao Tian, Wenhua Li *, Xiaohan Liu and Yongkun Wang

School of Electro-Mechanical Engineering, Xidian University, Number 2 Taibai South Road, Xi'an 710071, China; wctian@xidian.edu.cn (W.T.); xiaohanliu@stu.xidian.edu (X.L.); ykwang@xidian.edu.cn (Y.W.)

* Correspondence: wenhuali_xidian@163.com; Tel.: +86-29-8820-2954

Academic Editor: Gang Wei

Received: 2 December 2016; Accepted: 5 January 2017; Published: 12 January 2017

Abstract: Due to the excellent electronic, optical, thermal, chemical, and mechanical properties of graphene, it has been applied in microdevices and nanodevices. However, there are some structural defects in graphene limiting its application in micro electromechanical systems (MEMS). These structural defects are inevitable during processing, and it is difficult to assess their effect on the micro/nano devices. Therefore, this communication used molecular dynamics to study the resonance properties of a nanoelectromechanical systems (NMES) resonator based on a graphene sheet with a single vacancy defect and edge defects. This communication focuses on three factors: vacancy types, external force, and temperature. The resonance frequencies of both types of graphene increased with external stress loading, and the resonance frequency of the graphene showed a clear step-shaped variation. Nonlinear deformation of the sheet occurred between resonant processes. When the external force was less than 15.91 nN, the resonance frequencies of the two types of graphene showed a consistent trend. The maximum frequency was up to 132.90 GHz. When the external force was less than 90 nN, the resonance frequencies of graphene with edge defects were greater and changed more rapidly. Temperature did not have a huge influence on the resonance frequencies of either type of graphene structure. The resonance frequencies of graphene with two different vacancy defects showed a consistent trend.

Keywords: graphene; vacancy; resonance frequency; biosensing

1. Introduction

Graphene—a novel low-dimensional nano-material where carbon atoms are arranged in a honeycomb-structure—is formed by a flat monolayer of carbon atoms [1]. Due to its outstanding mechanical and electrical properties [2–5], graphene has broad application prospects, such as micro–nano devices [6–8], reinforcing materials, and photoelectric detection. In 2011, Min et al. [9] investigated a fast and reliable deoxyribonucleic acid (DNA) sequencing device. The feasibility of DNA sequencing using a fluidic nanochannel functionalized with a graphene nanoribbon was theoretically demonstrated. In 2014, Rajan et al. [10] found that the electron transmission of a graphene nanoribbon on which a molecule is adsorbed shows molecular fingerprints of Fano resonances, which can be used to devise an ultrasensitive Fano-resonance-driven DNA sequencing method. In addition, one research hotspot is the high frequency NEMS (nanoelectromechanical systems) graphene resonator, which shows potential for mass, charge, and force sensitivity [11,12]. In 2007, Bunch et al. [6] fabricated a graphene-based resonator via a suspended graphene nanoribbon above predefined trenches etched into a SiO₂ surface. The resonant properties of the monolayer and multilayer graphene were analyzed. The graphene sample showed few defects when it was exfoliated from graphite [13]. Recently,

graphene was chemically synthesized with no defects [14]. However, in most cases, a variety of imperfections—including vacancy defects [15,16], topological defects [17,18], adatom [19,20] and grain boundaries [21]—are inevitably produced during material processing. Because the mechanical and electrical properties of graphene are very sensitive to lattice imperfections [22], it is critically important to study defects in graphene [23]. In 2008, Meyer et al. observed graphene membranes with single atomic vacancy defects and edge defects through transmission electron microscopy, as is shown in Figure 1 [24].

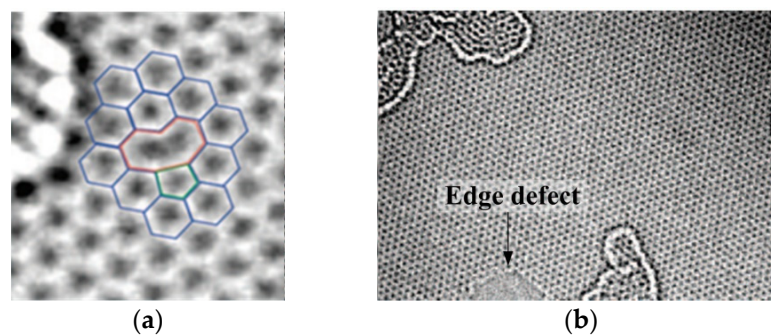


Figure 1. Experimental transmission electron microscope (TEM) image of (a) a single vacancy defect; and (b) an edge defect. Reproduced with permission from [24], © American Chemical Society, 2008.

It is noted that the experimental methods for the study of the vibrational properties of graphene sheets are very difficult. In order to be observed, graphene should be adsorbed on a substrate, which affects the original characteristic of graphene. However, the use of computer numerical simulation based on molecular dynamics (MD) [25] can overcome the difficulties of experimentation. Kim et al. [26] investigated the intrinsic loss mechanisms of monolayer graphene nanoresonators undergoing flexural oscillations via classical MD simulations. Jiang et al. [27] investigated edge effects on the quality factor of graphene nanoresonators with different edge configurations and of various sizes by MD. Zhan et al. [28] carried out a fundamental study of the vibrational performance of Ag nanowires (NW) by MD simulation. In this communication, MD has been employed to study the resonance pattern of graphene sheets with vacancy defects, based on a micro-resonator. The effects of defect location, stress, and environmental temperature of graphene on the resonance properties are discussed.

2. Physical Models and Simulation Methods

2.1. Modeling

Perfect graphene is a flat monolayer formed by single-layer hexagonal cellular carbon atoms. The length between two carbon atoms is $\sim 1.42 \text{ \AA}$. In this simulation, the graphene sheet was applied to an electromechanical resonator (Figure 2). Nano-resonators based on graphene sheets can be extremely fast and sensitive to reflect the changes in the tested factors. So, they have great potential and advantages in the field of clinical laboratory diagnosis. They use the resonance properties of graphene sheets to achieve energy conversion and sensing. When the surface mass load of the graphene sheet changes slightly, the resonant frequency can change significantly. Additionally, it can detect biological macromolecules which react specifically with immobilized probe molecules on the graphene surface substance. There are two types of defects in graphene sheets: single atomic vacancy defects (Figure 3a) and edge defects (Figure 3b). The dimension of the simulation model was $l = 30.06 \text{ nm} \times w = 4.05 \text{ nm}$. The thickness was the interlayer spacing of graphite, which is 0.335 nm . The whole graphene nanosheet was composed of 4828 carbon atoms. The graphene has to be suspended over a SiO_2 substrate in the actual resonator, so the two ends of the graphene sheet structure were fixed in the simulation. The actual oscillating length of the nanosheet was 27.56 nm . The atom vacancies were created by removing carbon atoms within the graphene sheets. The central atom A ($15.13 \text{ nm}, 1.96 \text{ nm}, 0 \text{ nm}$),

boundary atom B (23.82 nm, 0 nm, 0 nm), atom C (23.89 nm, −0.12 nm, 0 nm), atom D (24.04 nm, −0.12 nm, 0 nm), and atom E (24.10 nm, 0 nm, 0 nm) were removed.

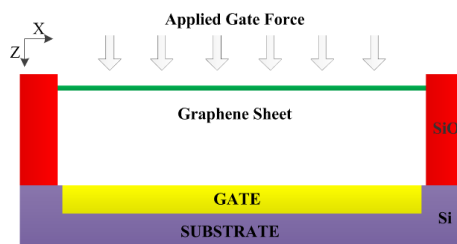


Figure 2. Model schematic of a graphene resonator.

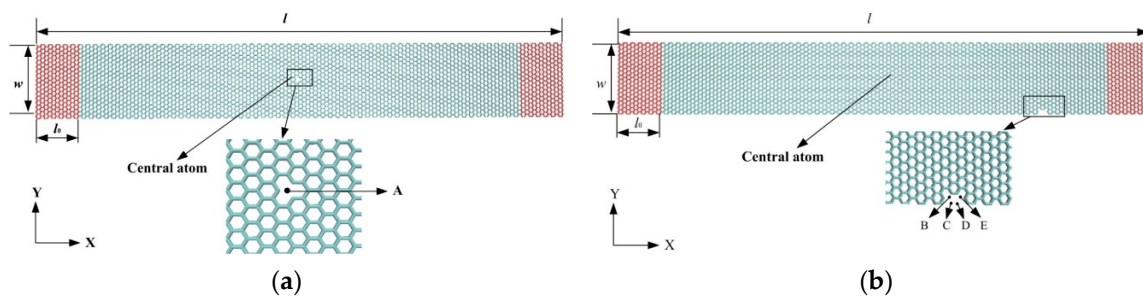


Figure 3. Simulation model of the graphene sheet with defects: (a) Single vacancy defect; (b) Edge defects.

2.2. Simulation Method and Process

The simulation was completed by large-scale atomic/molecular massively parallel simulator (LAMMPS) open source molecular dynamic software (version 15 May 2015, Sandia National Laboratories, Albuquerque, NM, USA). The adaptive intermolecular reactive empirical bond order potential (AIREBO) potential function was adopted to model the inter-atomic forces of carbon in the graphene. We used the Velocity–Verlet algorithm, the canonical ensemble (NVT), and a Nose–Hoover thermostat to control the temperature. The MD time step was 1×10^{-3} ps or 1 fs. Thirty thousand time steps were carried out during the relaxation, and the size of the cut-off radius was 10.2 Å. A periodic boundary condition was imposed in the x - and y -directions. The non-periodic boundary condition was imposed in the z -direction.

3. Results and Analysis

3.1. Influence of Different Forces on the Resonance Properties of Graphene with Vacancies

In this communication, the total energy of the system is analyzed to determine whether a stable equilibrium state is obtained. In this simulation, the relative variation of the total energy is output. According to processing and counting output data, the relationship between the total energy and time can be obtained. As Figure 4 shows, the total energy of the system in the initial relaxation time changes to some degree. With the increase of the relaxation time, the total energy fluctuates on a small scale. After that, the system reached a stable equilibrium state.

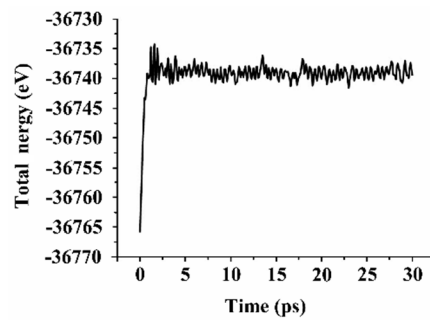


Figure 4. Relationship between total energy and relaxation time of grapheme.

The graphene nano resonator is generally driven by an electrostatic capacitive force induced by the potential difference between the graphene sheet and the gate [6,8]. So, in this simulation, the magnitude of the external force is calculated by the formula (1):

$$F = \frac{\partial W}{\partial d_0} = -\frac{\epsilon abU^2}{2d_0} \quad (1)$$

where F is the electrostatic force between two plate electrodes; W , d_0 are the energy and distance between the two plate electrodes, respectively; U is the voltage loaded between the two plate electrodes; and a , b are the length of the plate electrodes. Different voltages are selected to obtain different magnitudes of stress. A uniform force is loaded perpendicularly on the surface of the graphene, except the fixed ends (Figure 5). The electrostatic force is evenly distributed on each atom in the graphene nanosheet [29]. The total force is $F = f \times N$, where f is the force applied to each atom of the graphene sheet, and N is the number of atoms in graphene's effective region. The applied indented forces were 1.77 nN, 7.07 nN, 15.92 nN, 28.29 nN, 44.20 nN, 63.65 nN, 86.64 nN, and 113.15 nN. In this communication, a Fourier transform was applied to obtain the resonant frequency of the graphene with two different vacancies by selecting the kinetic energy of the system as the time-domain signal [30]. When the graphene is subjected to a certain load, the potential energy of the system will change accordingly. After 20,000 time steps, the load applied to the graphene was removed. The graphene structure will recover to the initial state due to the C-C bonds inside the graphene structure. At this point, the potential energy of the graphene will be converted to kinetic energy, and the graphene structure will oscillate. When the kinetic energy and potential energy of graphene were converted to each other, the graphene structure undergoes free vibration. During oscillation, 250,000 time steps or 250 ps were carried out. Figure 6 shows the amplitude versus frequency curve of the graphene sheet with a single defect. Figure 7 shows the function of resonance frequency of external force with two different vacancy defects.

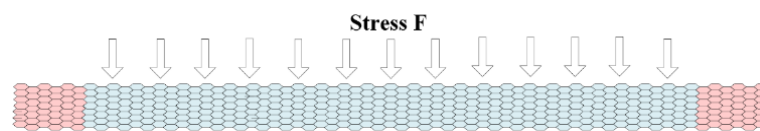


Figure 5. Schematic diagram of stress loading on the graphene structure.

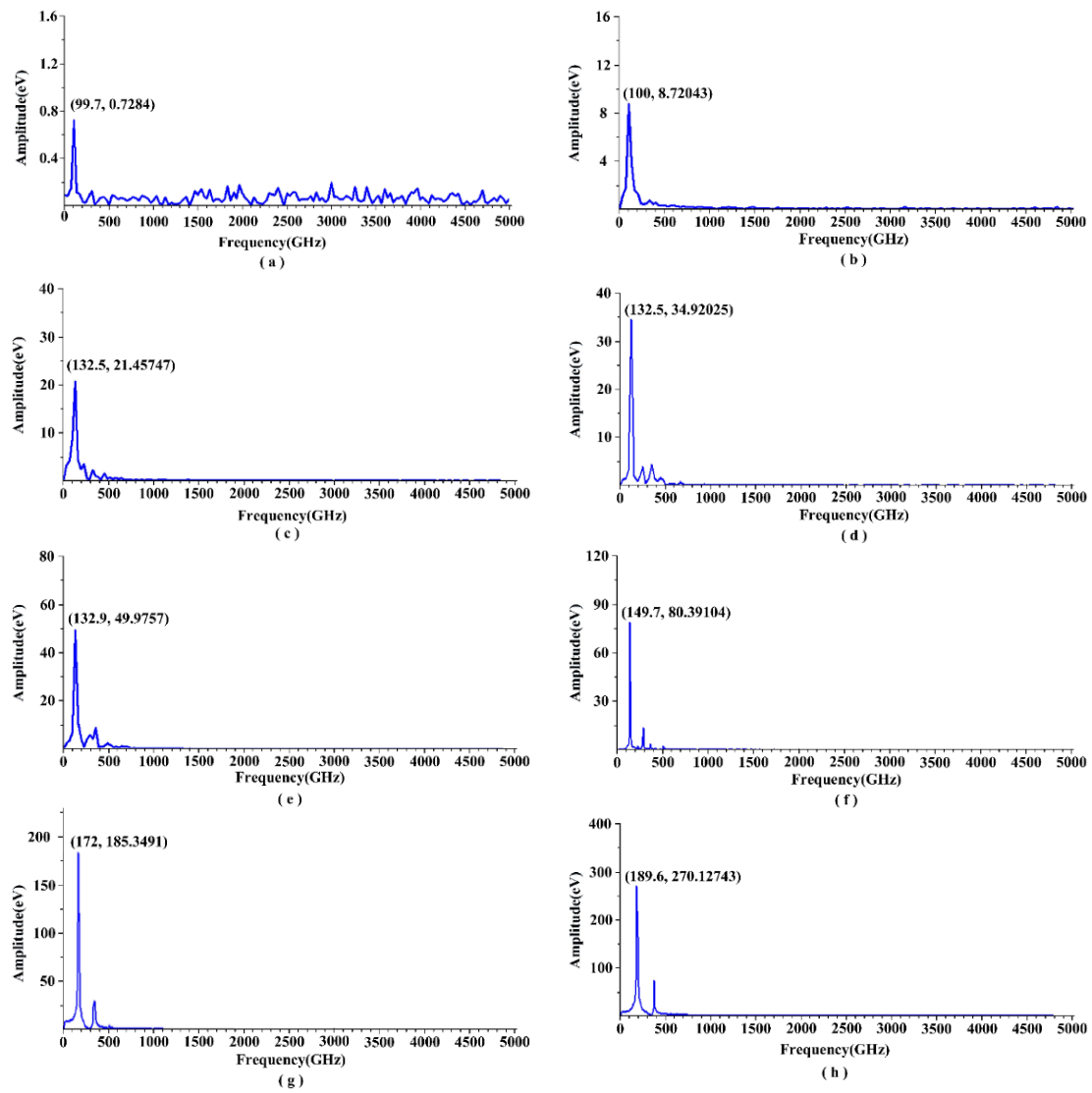


Figure 6. Amplitude versus frequency for external forces of (a) 1.768 nN; (b) 7.072 nN; (c) 15.912 nN; (d) 28.288 nN; (e) 44.2 nN; (f) 63.648 nN; (g) 86.638 nN; and (h) 113.152 nN.

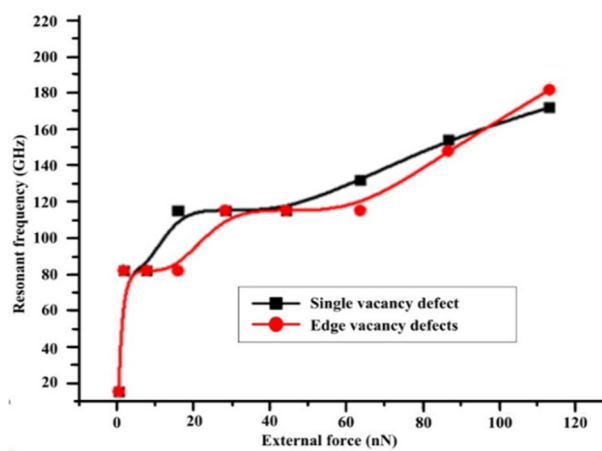


Figure 7. Resonance frequency as a function of external force with two different vacancy defects.

As shown in Figure 6, the resonance frequencies of both two types of graphene increase with increasing external stress loading. Additionally, the frequency shows a clear step-shaped variation, indicating that the dynamic behavior of graphene is dominated by nonlinear effects. The fundamental cause is the nonlinear deformation of the sheet between resonant processes [31]. Actually, based on thin plate theory, only when the deflection extremum value is much less than the thickness of the thin plate can linear theory describe the mechanical response process of the thin plate. This result is in good agreement with the literature [32]. As for a single-layered graphene sheet, its thickness is only 0.335 nm, so the linear response range is narrow. In other words, the resonance behavior of nanoscale systems is different from the resonance behavior of macroscopic systems. When the external force is less than 15.91 nN, the resonance frequencies of both types of graphene structure show a consistent trend. The maximum frequency is 132.9 GHz. When the external force was less than 90 nN, the resonance frequencies of graphene with a single vacancy defect were greater than the resonance frequencies of graphene with edge defects. When the external force was less than 90 nN, the resonance frequencies of graphene with edge defects was greater and changed more rapidly. In this regard, a defect-driven resonator may be useful to identify such defects.

In order to more accurately analyze the vibration process, the central atom of the graphene sheet was tracked. Absolute displacement of the tracking atom in the normal direction under different external loading is shown in Figure 8. It can be inferred that the graphene sheet demonstrated a sinusoidal periodic vibration process. Under the effects of different external forces, the amplitude and the vibration period of the graphene were different. As the stress increased, the amplitude of the graphene showed an increasing tendency.

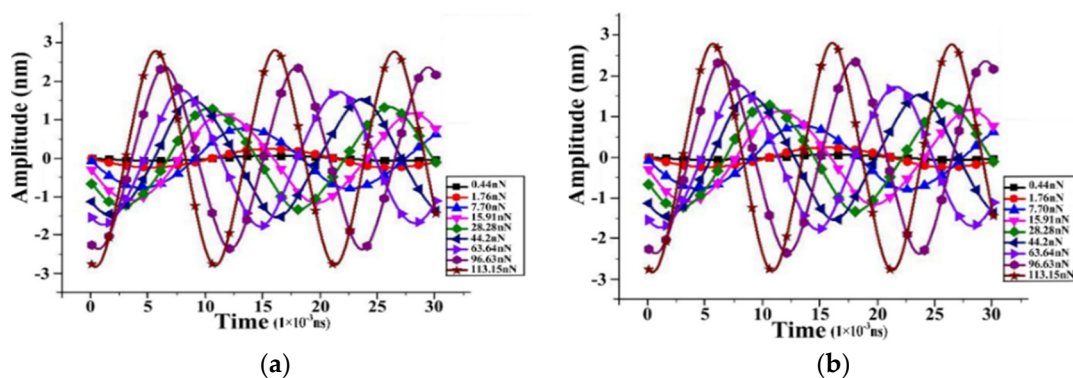


Figure 8. Absolute displacement of central atom in the normal direction with different external loading: (a) Single vacancy defect; (b) Edge defects.

3.2. Influence of Different Temperature on the Resonance Properties of Graphene with Vacancies

First, a full relaxation should be completed; the system temperature was set to 0.1 K, 50 K, 75 K, 100 K, 200 K, 400 K, 600 K, 800 K, and 1000 K, respectively. When the relaxation was finished, a force of 15.91 nN in stress was loaded. Figure 7 shows the resonance frequencies of two different graphene sheets with vacancy as a function of system temperature.

As is shown in Figure 9, the resonance frequencies of the two types of graphene structure show a consistent trend with different temperature conditions. Actually, the resonance frequencies of edge defects are 0.5 GHz lower than that of a single vacancy. The curve is fitted, so there is little difference in the graph. We suspect that this phenomenon is due to the small amount of defects. The resonance frequencies had a step-by-step jump increase between 50 K and 75 K. The resonance frequencies jumped to 132.9 GHz at point N in Figure 9. Chen [8] and Singh [33] investigated the effect of temperature on the resonant frequencies of the graphene resonators clamped on two edges. It was found that the change in temperature resulted in an expansion/contraction reaction between the substrate and the graphene beam, leading to an increase in thermal stress. It was also found that the stress in the graphene film

increased the resonant frequency. Furthermore, during the free vibration process, statistical analysis was conducted on the motion state of the central atom A (Figure 10). Both types of graphene structure demonstrated a sinusoidal periodic vibration process. Under different temperatures, the amplitude and the vibration periods of the graphene were different. The amplitudes of the graphene increased with increasing temperature.

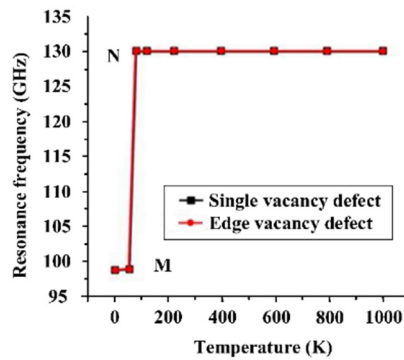


Figure 9. Resonance frequency as a function of temperature with two different vacancy defects.

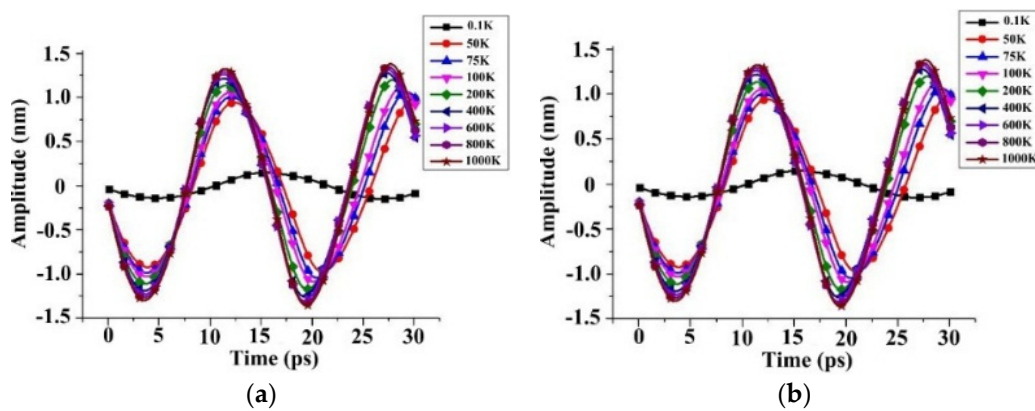


Figure 10. Absolute displacement in the normal direction at different system temperatures: (a) Single vacancy defect; (b) Edge defects.

4. Conclusions

In this communication, the resonant properties of graphene sheets with different types of vacancies was investigated by molecular dynamics simulation. The effect of defect type, external stress, and system temperature on the resonance properties of graphene have been discussed. The resonance frequencies of both types of graphene increased with external stress loading. It shows a clear step-shaped variation. This is mainly due to the occurrence of nonlinear deformations of graphene in the vibration process. When the external force is less than 15.91 nN, the resonance frequencies of two types of graphene showed a consistent trend. The maximum frequency was up to 132.9 GHz. When the external force was less than 90 nN, the resonance frequencies of graphene with a single vacancy defect were greater than the resonance frequencies of graphene with edge defects. When the external force was less than 90 nN, the resonance frequencies of graphene with edge defects were greater and changed more rapidly. Temperature had little influence on the resonance frequency of the graphene nanosheet. The resonance frequency was 99.7 GHz between 0.1 K and 50 K. When the temperature was 75 K, the resonance frequency jumped to 132.9 GHz. When the temperature was greater than 75 K, the resonance frequency remained constant. Due to the ultralow density, ultrahigh resonance frequency, high strength and stiffness, high sensitivity to the environment, and other

characteristics, graphene can be considered as an ideal material for ultra-sensitive biosensors which can achieve accurate and highly-selective detection of biomolecules.

Acknowledgments: The work is supported by Research Program supported by National Science Foundation of China (61176130) and National Science Foundation of Ningbo (2016A610030).

Author Contributions: W.T. conceived and designed the experiments; W.L., X.L. and Y.W. performed the experiments and analyzed the data; W.L. wrote the paper.

Conflicts of Interest: The authors declare no conflict of interest.

References

1. Novoselov, K.S.; Geim, A.K.; Morozov, S.V. Electric field effect in atomically thin carbon films. *Science* **2004**, *306*, 666–669. [[CrossRef](#)] [[PubMed](#)]
2. Sandoz-Rosado, E.J.; Tertuliano, O.A.; Terrell, E.J. An atomistic study of the abrasive wear and failure of graphene sheets when used as a solid lubricant and a comparison to diamond-like-carbon coatings. *Carbon* **2012**, *50*, 4078–4084. [[CrossRef](#)]
3. Bao, Q.; Loh, K.P. Graphene photonics, plasmonics, and broadband optoelectronic devices. *ACS Nano* **2012**, *6*, 3677–3694. [[CrossRef](#)] [[PubMed](#)]
4. Tian, W.C.; Zhang, X.Y.; Chen, Z.Q.; Ji, H.Y. A review of graphene on NEMS. *Recent Pat. Nanotechnol.* **2015**, *10*, 3–10. [[CrossRef](#)]
5. Xie, S.X.; Jiao, N.D.; Tung, S.; Liu, L.Q. Fabrication of SWCNT-graphene field-effect transistors. *Micromachines* **2016**, *6*, 1317–1330. [[CrossRef](#)]
6. Bunch, J.S.; van der Zande, A.M.; Verbridge, S.S.; Frank, I.W.; Tanenbaum, D.M. Electromechanical resonators from graphene sheets. *Science* **2007**, *315*, 490–493. [[CrossRef](#)] [[PubMed](#)]
7. Frank, I.W.; Tanenbaum, D.M.; Zande, A.M.V.D.; Mceuen, P.L. Mechanical properties of suspended graphene sheets. *J. Vac. Sci. Technol. B* **2007**, *25*, 2558–2561. [[CrossRef](#)]
8. Lee, J.; Wang, Z.; He, K.; Shan, J.; Feng, P.X. High frequency MoS₂ nanomechanical resonators. *ACS Nano* **2013**, *7*, 6086–6091. [[CrossRef](#)] [[PubMed](#)]
9. Min, S.K.; Kim, W.Y.; Cho, Y.; Kim, K.S. Fast DNA sequencing with a graphene-based nanochannel device. *Nat. Nanotechnol.* **2011**, *6*, 162–165. [[CrossRef](#)] [[PubMed](#)]
10. Rajan, A.C.; Rezapour, M.R.; Yun, J.; Cho, Y.; Cho, W.J.; Min, S.K.; Lee, G.; Kim, K.S. Two Dimensional Molecular Electronics Spectroscopy for Molecular Fingerprinting, DNA Sequencing, and Cancerous DNA Recognition. *ACS Nano* **2014**, *8*, 1827–1833. [[CrossRef](#)] [[PubMed](#)]
11. Wei, Y.; Zhan, H.; Xia, K.; Zhang, W.; Sang, S.; Gu, Y. Resonance of graphene nanoribbons doped with nitrogen and boron: A molecular dynamics study. *Beilstein J. Nanotechnol.* **2014**, *5*, 717–725. [[CrossRef](#)] [[PubMed](#)]
12. Zhan, H.F.; Zhang, Y.Y.; Bell, J.M.; Zhang, B.C.; Gu, Y.T. Tailoring the Resonance of Bilayer Graphene Sheets by Interlayer sp³ Bonds. *J. Phys. Chem. C* **2014**, *118*, 732–739. [[CrossRef](#)]
13. Kim, K.S.; Zhao, Y.; Jang, H.; Lee, S.Y.; Kim, J.M.; Kim, K.S.; Ahn, J.H.; Kim, P.; Choi, J.Y.; Hong, B.H. Large-scale pattern growth of graphene films for stretchable transparent electrodes. *Nature* **2009**, *457*, 706–710. [[CrossRef](#)] [[PubMed](#)]
14. Cai, J.; Ruffieux, P.; Jaafar, R.; Bieri, M.; Braun, T.; Blankenburg, S.; Muoth, M.; Seitsonen, A.P.; Saleh, M.; Feng, X.; et al. Atomically precise bottom-up fabrication of graphene nanoribbons. *Nature* **2010**, *466*, 470–473. [[CrossRef](#)] [[PubMed](#)]
15. Chang, S.; Zhang, Y.; Huang, Q.; Wang, H.; Wang, G. Effects of vacancy defects on graphene nanoribbon field effect transistor. *IET Micro Nano Lett.* **2013**, *8*, 816–821. [[CrossRef](#)]
16. Deretzi, I.; Fiori, G.; Iannaccone, G.; Magna, A.L. Effects due to backscattering and pseudogap features in graphene nanoribbons with single vacancies. *Phys. Rev. B* **2010**, *81*, 085427. [[CrossRef](#)]
17. Stone, A.J.; Wales, D.J. Theoretical studies of icosahedral C₆₀ and some related species. *Chem. Phys. Lett.* **1986**, *128*, 501–503. [[CrossRef](#)]
18. Xu, S.C.; Irle, S.; Musaev, D.G.; Lin, M.C. Quantum chemical prediction of reaction pathways and rate constants for dissociative adsorption of CO(x) and NO(x) on the graphite (0001) surface. *J. Phys. Chem. B* **2006**, *110*, 21135–21144. [[CrossRef](#)] [[PubMed](#)]

19. Lehtinen, P.O.; Foster, A.S.; Ayuela, A.; Krasheninnikov, A.; Nordlund, K.; Nieminen, R.M. Magnetic properties and diffusion of adatoms on a graphene sheet. *Phys. Rev. Lett.* **2003**, *91*, 017202. [[CrossRef](#)] [[PubMed](#)]
20. Talapatra, S.; Ganesan, P.G.; Kim, T.; Vajtai, R.; Huang, M.; Shima, M.; Ramanath, G.; Srivastava, D.; Deevi, S.C.; Ajayan, P.M. Irradiation-induced magnetism in carbon nanostructures. *Phys. Rev. Lett.* **2005**, *95*, 097201. [[CrossRef](#)] [[PubMed](#)]
21. Yu, S.U.; Park, B.; Cho, Y.; Hyun, S.; Kim, J.K.; Kim, K.S. Simultaneous Visualization of Graphene Grain Boundaries and Wrinkles with Structural Information by Gold Deposition. *ACS. Nano* **2014**, *8*, 8662–8668. [[CrossRef](#)] [[PubMed](#)]
22. Son, Y.W.; Cohen, M.L.; Louie, S.G. Half-metallic graphene nanoribbons. *Nature* **2006**, *444*, 347–349. [[CrossRef](#)] [[PubMed](#)]
23. Qi, Z.; Park, H.S. Intrinsic energy dissipation in CVD-grown graphene nanoresonators. *Nanoscale* **2012**, *11*, 3460–3465. [[CrossRef](#)] [[PubMed](#)]
24. Meyer, J.C.; Kisielowski, C.; Erni, R.; Rossell, M.D.; Crommie, M.F.; Zettl, A. Direct imaging of lattice atoms and topological defects in graphene membranes. *Nano Lett.* **2008**, *8*, 3582–3586. [[CrossRef](#)] [[PubMed](#)]
25. Neekamal, M.; Peeters, F.M. Linear reduction of stiffness and vibration frequencies in defected circular monolayer graphene. *Phys. Rev. B* **2010**, *23*, 5032.
26. Kim, S.Y.; Park, H.S. The importance of edge effects on the intrinsic loss mechanisms of graphene nanoresonators. *Nano Lett.* **2009**, *9*, 969–974. [[CrossRef](#)] [[PubMed](#)]
27. Jiang, J.W.; Wang, J.S. Why edge effects are important on the intrinsic loss mechanisms of graphene nanoresonators. *J. Appl. Phys.* **2012**, *111*, 054314–054319. [[CrossRef](#)]
28. Zhan, H.F.; Gu, Y.T. A fundamental numerical and theoretical study for the vibrational properties of nanowires. *J. Appl. Phys.* **2012**, *111*, 124303–124309. [[CrossRef](#)]
29. Kang, J.W.; Kim, H.W.; Kim, K.S.; Lee, J.H. Molecular dynamics modeling and simulation of a graphene-based nanoelectromechanical resonator. *Curr. Appl. Phys.* **2013**, *13*, 789–794. [[CrossRef](#)]
30. And, F.H.; Kasemo, B.; Nylander, T.; Fant, C.; Kristin Sott, A.; Elwing, H. Variations in coupled water, viscoelastic properties, and film thickness of a mefp-1 protein film during adsorption and cross-linking: A quartz crystal microbalance with dissipation monitoring, ellipsometry, and surface plasmon resonance study. *Anal. Chem.* **2001**, *73*, 5796–5804.
31. Banhart, F.; Kotakoski, J.; Krasheninnikov, A.V. Structural defects in graphen. *ACS Nano* **2011**, *5*, 26–41. [[CrossRef](#)] [[PubMed](#)]
32. Gu, F.; Zhang, J.H.; Yang, L.J.; Gu, B. Molecular dynamics simulation of resonance properties of strain graphene nanoribbons. *Acta Phys. Sin.* **2011**, *60*, 056103.
33. Singh, V.; Sengupta, S.; Solanki, H.S.; Dhall, R.; Allain, A.; Dhara, S.; Pant, P.; Deshmukh, M.M. Probing thermal expansion of graphene and modal dispersion at low-temperature using graphene nanoelectromechanical systems resonators. *Nanotechnology* **2010**, *21*, 165204–165211. [[CrossRef](#)] [[PubMed](#)]

